

## An Adaptive Cracking Particle Method for 2D Crack Propagation

Weilong Ai\*, Charles E. Augarde

*School of Engineering and Computing Sciences, Durham University, DH1 3LE, United Kingdom*

### SUMMARY

(TO BE REVISED ONCE TEXT IS COMPLETE) An adaptive Cracking Particle Method is developed to model the crack propagation process. A set of cracking particles are used to describe the crack patterns and can be easily updated when the crack propagates. The change of cracking angle is recorded in discrete segments of broken lines which makes this methodology suitable to model discontinuous cracks. The node arrangements can be set up automatically by the adaptivity approach throughout the whole propagation steps to keep the accuracy and efficiency of the analysis. The system stiffness is calculated and stored in local matrices, so only a small influenced domain should be recalculated for each step while the remainder can be read directly from the storage, which greatly reduces the computational expense. The methodology is applied to several 2D crack problems and good agreements are achieved. Copyright © 2015 John Wiley & Sons, Ltd.

Received . . .

KEY WORDS: Adaptivity, CPM, EFG, crack propagation, meshless methods

---

\*Correspondence to: School of Engineering and Computing Sciences, Durham University, DH1 3LE, United Kingdom

## 1. INTRODUCTION

Despite the antiquity of the problem of engineering fracture, its modelling remains a key research topic in computational solid mechanics as it challenges numerical methods which have proved more than adequate for other applications. The traditional finite element method (FEM) has been adapted for fracture modelling into interelement separation methods where a crack is allowed to propagate along defined paths (interelement edges) [1, 2]. However, results have been shown to strongly depend on the shape and orientation of meshes, and there is an overestimation of the fracture energy when the actual crack path is not along interelement edges. The Extended FEM (XFEM) models cracks embedded inside elements without reference to the mesh arrangement via an enrichment that accounts for the discontinuity at the crack face. This, however, requires an explicit description of the crack pattern, which is often provided by a signed distance function or equivalent level sets, as in [3, 4, 5, 6, 7], an approach that becomes cumbersome when considering problems with many cracks. Meshless methods, which discretise on the basis of nodes alone, largely remove the link to a predefined mesh met with standard FEMs and also deliver solutions to other problems such as mesh distortion and volumetric locking and it is no surprise that they have been applied with vigour to fracture problems for 20 years [8, 9, 10]. More recently meshless methods have been combined with explicit crack descriptions, again using level sets (e.g. [6, 7]), although with the same issues as mentioned above for the XFEM. In 2004 the Cracking Particle Method (CPM) was presented in [11] as an alternative and pragmatic approach to meshless modelling of fracture, where the crack path is not represented explicitly but instead in an approximate manner by the use of nodes which are deemed “cracked”; the locations of the collection of cracked nodes being an approximation for the crack path (or paths). While the CPM makes it easy to update cracks by adding or deleting cracking particles, fine nodal arrangements are required to accurately simulate crack patterns and to obtain accurate stress intensity factors.

In this paper a modified CPM is presented which improves modelling of curved crack paths and also addresses the issue of accuracy by incorporating adaptivity. The method is demonstrated for the case of linear elastic fracture mechanics problems in 2D but extension to cohesive cracking and to 3D is conceptually trivial. The structure of this paper is as follows: the background governing equations for the modelling are given in Section 2 followed by a more detailed description (in Section 3) of the original CPM and the crack propagation criterion used. The adaptive approach is described in Section 4, and some numerical examples are provided in Section 5 to explore the performance of the proposed methodology.

## 2. GOVERNING EQUATIONS AND APPROXIMATION FRAMEWORK

We consider the following two dimensional (2D) problem in the domain  $\Omega$  with boundary  $\Gamma$ . The strong form of the equilibrium equation is

$$\nabla \cdot \boldsymbol{\sigma} + \mathbf{b} = \mathbf{0} \quad \text{in } \Omega \quad (1)$$

with boundary conditions

$$\boldsymbol{\sigma} \cdot \mathbf{n} = \bar{\mathbf{t}} \quad \text{on } \Gamma_t, \quad (2)$$

$$\mathbf{u} = \bar{\mathbf{u}} \quad \text{on } \Gamma_u, \quad (3)$$

where  $\boldsymbol{\sigma}$  and  $\mathbf{u}$  are the stress tensor and displacement vector respectively and  $\mathbf{b}$  is the vector of body forces (if present).  $\mathbf{n}$  is the unit normal to the domain  $\Omega$ ,  $\bar{\mathbf{t}}$  and  $\bar{\mathbf{u}}$  are traction and displacement constraints on the boundary  $\Gamma$  with  $\Gamma = \Gamma_t \cup \Gamma_u$ .

The CPM uses the Element-Free Galerkin method (EFGM) to discretise a weak form of Eqns 1 to 3 [12, 13]. The approximate displacement at location  $\mathbf{x}$  in  $\Omega$ ,  $u^h(\mathbf{x})$  is given by a

linear combination of shape functions  $\Phi_i(\mathbf{x})$  and nodal displacements  $u_i$  as

$$w^h(\mathbf{x}) = \sum_{i=1}^n \Phi_i(\mathbf{x})u_i = \mathbf{\Phi}^T \mathbf{u}, \quad (4)$$

where  $i$  is the node index with coordinate  $\mathbf{x}_i$  and  $n$  is the number of nodes within  $\Omega$ . The shape functions  $\Phi_i(\mathbf{x})$  are determined via a moving least squares (MLS) approximation, defined by a basis vector  $\mathbf{p}(\mathbf{x}_i)$  and weight functions  $w_i(\mathbf{x} - \mathbf{x}_i)$  as

$$\mathbf{\Phi}(\mathbf{x}) = \mathbf{p}^T(\mathbf{x})\mathbf{A}(\mathbf{x})^{-1}\mathbf{B}(\mathbf{x}), \quad (5)$$

where

$$\mathbf{A}(\mathbf{x}) = \sum_i^n w_i(\mathbf{x} - \mathbf{x}_i)\mathbf{p}^T(\mathbf{x}_i)\mathbf{p}(\mathbf{x}_i), \quad (6)$$

and

$$\mathbf{B}(\mathbf{x}) = [w_1(\mathbf{x} - \mathbf{x}_1)\mathbf{p}(\mathbf{x}_1), w_2(\mathbf{x} - \mathbf{x}_2)\mathbf{p}(\mathbf{x}_2), \dots, w_n(\mathbf{x} - \mathbf{x}_n)\mathbf{p}(\mathbf{x}_n)]. \quad (7)$$

Generally, the weight functions  $w_i(\mathbf{x} - \mathbf{x}_i)$  are chosen as positive so that the  $\mathbf{A}$  matrix is positive definite, and also to decrease with the distance between  $\mathbf{x}$  and  $\mathbf{x}_i$  due to the fact that the node  $i$  should be influenced more by nearer nodes. A small domain  $\Omega_i$  is defined and associated with node  $i$  outside of which the weight function  $w_i(\mathbf{x} - \mathbf{x}_i)$  is zero. A point in the domain is *supported* by nodes for which the weight function is non-zero at that location. A typical weight function (a quartic spline) is

$$w_i(\mathbf{x} - \mathbf{x}_i) = w(s) = \begin{cases} 1 - 6s^2 + 8s^3 - 3s^4 & \text{if } s \leq 1 \\ 0 & \text{if } s > 1, \end{cases} \quad (8)$$

where

$$s = \frac{\|\mathbf{x} - \mathbf{x}_i\|}{R_i}. \quad (9)$$

These weight functions have radial symmetry in  $\mathbf{x}$  where  $R_i$  is the influence domain radius of node  $i$  (a user defined parameter) and  $\|\cdot\|$  is the  $L_2$  norm. Many other weight functions have been proposed in the many EFGM references, e.g. [12, 8, 9, 13]. The essential boundary conditions cannot be imposed directly in the EFGM due to the non-interpolatory nature of the MLS approximation and in common with many other references, here Lagrange Multipliers are used. Further mathematical details of the conversion to the weak form, the moving least squares approximation used in the EFGM and the imposition of essential boundary conditions using Lagrange multipliers is contained in many other papers and is not repeated here.

### 3. A NEW CRACKING PARTICLES METHOD

The original CPM was introduced in 2004 by Rabczuk [11] who later extended it to 3D and to large deformation problems [14, 15]. It is fair to say that since its introduction the CPM has not had the same level of interest as enrichment-type methods for meshless fracture, but a number of papers have appeared recently applying CPM to dynamic fracture [16], the use of obscuration zones [17], ductile fracture [18, 19] and in [20] some issues associated with integration have been addressed using stabilized nodal methods.

Fig. 1 shows the CPM concept. In all versions of the CPM, the  $\mathcal{N}$  nodes in the domain  $\Omega$  are divided into two groups: cracking particles  $\mathcal{N}_c$  and normal particles  $\mathcal{N}_n$ . Displacement is continuous in  $\Omega$  but discontinuous at the crack. (By comparison, in the XFEM the crack is independent of the nodes and elements and is represented in a continuous fashion). In the original CPM the crack was modelled by a set of discrete line segments, which are restricted

to pass through meshless nodes (or “particles”) [11] and additional unknowns were introduced into the formulation to simulate the displacement discontinuity at the crack passing through the particle. A later CPM dispenses with this by splitting each particle into two new particles when a crack is to be modelled [15]. The difference being this and the original approach is shown in Figs. 2A and 2B. Cracking particles are split into two parts located on the opposite sides  $\mathcal{S}^+$  and  $\mathcal{S}^-$  of the crack segment and the crack opening displacement becomes

$$\llbracket u(\mathbf{x}) \rrbracket = \sum_{i \in \mathcal{S}^+} \Phi_i(\mathbf{x}^+) u_i + \sum_{i \in \mathcal{S}^-} \Phi_i(\mathbf{x}^-) u_i \quad (10)$$

where  $\llbracket \cdot \rrbracket$  stands for the distance between a pair of cracking particles,  $\mathbf{x}^+$  and  $\mathbf{x}^-$  are nodes located in opposite sides  $\mathcal{S}^+$  and  $\mathcal{S}^-$  respectively. In this work, the CPM of Fig. 2B is amended

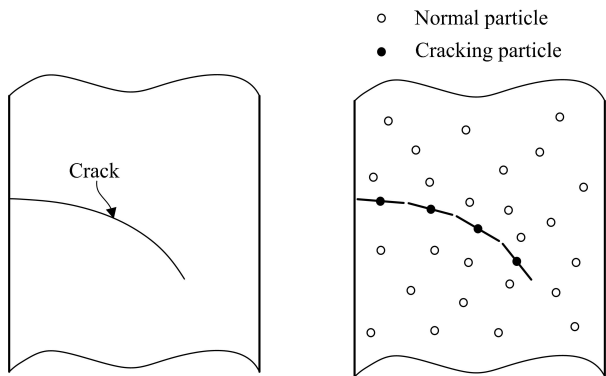


Figure 1. The original cracking particle method with straight crack segments at cracked nodes

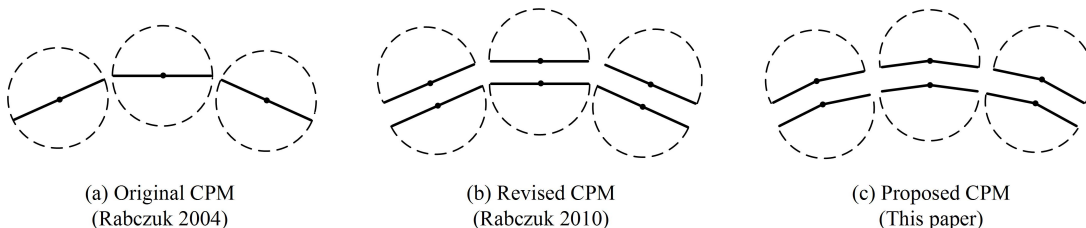


Figure 2. The development of the CPM

to allow better representation of curved cracks, by splitting the crack segment associated with a particle into two linear sections, as shown in Fig. 2C. The nodal support is split into two sectors according to the crack pattern where, for a given cracking particle  $i$ , the two segment arm directions are defined by angles  $\theta_1^i, \theta_2^i$  where  $\theta \in (-\pi, \pi]$  and

$$\theta_1^i = \arctan\left(\frac{y_{i+1} - y_i}{x_{i+1} - x_i}\right), \quad \theta_2^i = \arctan\left(\frac{y_{i-1} - y_i}{x_{i-1} - x_i}\right), \quad i \in \mathcal{N}_c. \quad (11)$$

The relationship is depicted in Fig. 3 (here *arctan* should be *atan2* in Matlab).

The crack tip location is influenced by nodes to both sides of the crack path, so is not itself split. This key difference between the original CPM and that proposed here is illustrated in Fig. 4. For a circular path, for example, the approximated path will be formed of tangents in the former method and chords in the latter method. For a fine nodal arrangement, both will approach the true path. However an advantage of the proposed method is that crack segments do not cross, a feature which can produce spurious cracking, a problem in the original CPM [15].

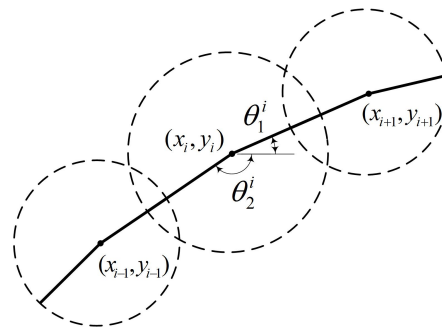


Figure 3. The two segment arm directions of a cracking particle

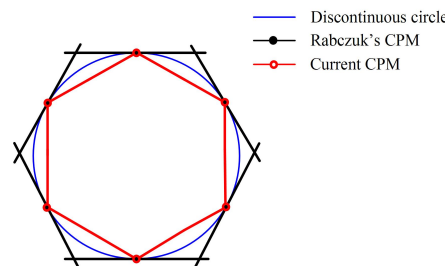


Figure 4. Comparison between current CPM and previous one

To capture the displacement jump along cracks in any meshless method, the supports of nodes adjacent to crack faces need adjustment, to avoid nodes on one side of a crack having influence over parts of the domain which are unconnected across the crack. There are two methods to fulfill this task: the visibility criterion [12] and the diffraction criterion [21]. In the visibility criterion, the modified support becomes the area receiving “light” from node  $i$  and ignores the part of support which is in the “shadow” caused by the discontinuity, as shown in Fig. 5. By contrast, the diffraction method takes a small part of the shadow into consideration akin to “ray diffraction” around the crack tip, which makes a more moderate truncation. The input parameter  $r_0 = \|\mathbf{x} - \mathbf{x}_i\|$  of the weight function  $w(\|\mathbf{x} - \mathbf{x}_i\|)$  is modified correspondingly as

$$r_0 = \left( \frac{\|\mathbf{x} - \mathbf{x}_i\| + \|\mathbf{x}_c - \mathbf{x}_i\|}{r_0} \right)^\gamma r_0 \tag{12}$$

where  $\mathbf{x}_c$  is the coordinate of the crack tip and  $\gamma$  is a constant for which a reasonable choice is 1 or 2 according to [21]. The diffraction method provides more accurate results than the visibility criterion, but becomes computationally complex when used for non-planar cracks in 3D or for multiple cracks in 2D and 3D, so the visibility criterion is employed in this paper (although without the additional tie elements proposed in [6] for simplicity).

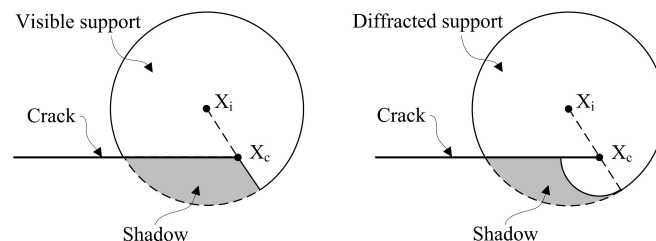


Figure 5. Visibility and diffraction criterion

### 3.1. SIFs and crack propagation

To complete the new CPM for fracture propagation two more components are required: a means to calculate Stress Intensity Factors (SIFs) and a rule for propagation direction. The well-known  $\mathcal{J}$  integral proposed by Rice [22], which is path-independent and therefore can be evaluated from far field results, is used here. The  $\mathcal{J}$  integral in 2D is defined by

$$\mathcal{J} = \int_{\Gamma} \left( W \, dy - \mathbf{T} \frac{\partial \mathbf{u}}{\partial x} \, ds \right), \quad (13)$$

(index notation used here which clashes with matrix-vector elsewhere. Can this be rewritten in matrix-vector?) where path  $\Gamma$  is a curve surrounding the crack tip, strain energy density is  $W = \frac{1}{2} \sigma_{ij} u_{i,j}$  and traction  $\mathbf{T}$  is  $T_i = \sigma_{ij} n_j$  defined according to the outward normal along  $\Gamma$ . The relationship between  $\mathcal{J}$  integral and the SIFs is

$$\mathcal{J} = \alpha(K_I^2 + K_{II}^2), \quad (14)$$

and

$$\alpha = \begin{cases} (1 - \nu^2)/E & \text{for plane strain,} \\ 1/E & \text{for plane stress,} \end{cases} \quad (15)$$

where  $E$  is the Young's modulus and  $\nu$  is the Poisson's ratio. (Is this section relevant if the J integral approach was used here?) (I think this part is to simply describe how to calculate the J integral.) There are generally two methods to calculate the  $\mathcal{J}$  integral: contour integrals [23, 24] and domain integrals [25]. The integral path for the contour integral usually follows a circle or a square around a crack tip (in 2D), but this method becomes complex for a kinked crack or for a mixed-mode problem. In contrast, the domain integral is a more general and is applicable to both linear and non-linear problems [26]. By applying the divergence theorem, the contour integral is converted into a domain form. In this domain, two independent equilibrium states of an elastically deformed body are considered, a real state  $u$  and an defined auxiliary state  $u^{aux}$  where the superscript implies the auxiliary state. The "so-called" interaction integral  $I$  of the superimposed state is

$$I = \int_A (\sigma_{ij}^{aux} u_{j,1} + \sigma_{ij} u_{j,1}^{aux} - \sigma_{jk}^{aux} \varepsilon_{jk} \delta_{1i}) q_{,i} \, dA, \quad i, j, k \in [1, 2], \quad (16)$$

where  $q$  is a predefined weight function with values varying from 1 on the domain boundary to 0 on the centre, and  $i, j$  and  $k$  are the index notation. The SIFs can be obtained through the relation below

$$I = 2\alpha(K_I K_I^{aux} + K_{II} K_{II}^{aux}), \quad (17)$$

where  $K_I^{aux}$  and  $K_{II}^{aux}$  are the SIFs associated with the auxiliary state and are defined initially. For instance, if  $K_I^{aux} = 1$  and  $K_{II}^{aux} = 0$  then  $K_I$  can be found by  $K_I = I/(2\alpha)$ . Further details of this method can be found in [25].

Different crack propagation criteria are discussed in [27], and the maximum principal stress criterion is the simplest but provides good results. This approach is employed here, which defines crack propagation direction as perpendicular to the maximum principal stress [28]. Thus, the crack growth angle  $\theta$  in the tip local polar coordinate system as in Fig. 6 (this should be indicated on a figure somewhere) is decided by setting the shear stress to zero so that

$$K_I \sin \theta + K_{II} (3 \cos \theta - 1) = 0. \quad (18)$$

Solving this gives

$$\theta = 2 \arctan \frac{1}{4} \left[ \frac{K_I}{K_{II}} - \text{sign}(K_{II}) \sqrt{\left(\frac{K_I}{K_{II}}\right)^2 + 8} \right]. \quad (19)$$

Then an increment is set up along  $\theta$  and a normal particle becomes cracking or a new cracking particle is introduced if there is no particle already there.

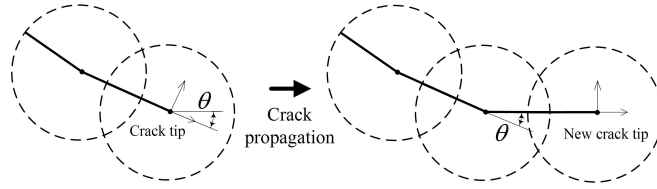


Figure 6. New cracking particle due to crack propagation

#### 4. ADDING ADAPTIVITY TO THE CPM

A major challenge for accurate computational modelling in linear elastic fracture mechanics is the stress singularity at the crack tip, and to a lesser extent, the high gradients of displacements close to the crack tip. In a meshless method, a large number of nodes, or a high order basis (or both), are required around a crack tip to achieve accurate results, but away from the crack tip there is rarely a need for the same level of refinement. Currently, how to set up the arrangement of nodes automatically to achieve a given level of accuracy is a challenge, particularly when there is crack propagation and an adaptive procedure is needed for efficiency.

*a posteriori* adaptive finite element methods, which comprise an error estimation step followed by an amendment to the discretisation of the problem, have a long history and a well-developed mathematical basis. For this class of adaptive methods most error estimators belong to two categories: recovery based [29, 30, 31, 32] or residual based [33, 34, 35]. Reviews on this topic can be found in [36, 37]. Three main strategies for amending the discretisation are: mesh refinement (*h*-adaptivity), increasing the polynomial degree of the shape functions (*p*-adaptivity) and the combination of the two (*hp*-adaptivity) [38]. All approaches have been tried with meshless methods over the years, e.g. [12, 39, 40, 29] but there is at present no firm mathematical basis for error estimators for meshless methods, indeed recent studies indicate that simply applying FEM-based adaptive approaches to meshless methods may be problematic [41].

In this study we supplement the new CPM described above with an adaptive capability using a recovery based error estimator computed in a convenient form based on the difference between the “exact” stress  $\boldsymbol{\sigma}$  and the calculated stress  $\boldsymbol{\sigma}^h$  using the error energy norm

$$\|e_\sigma\| = \left\{ \frac{1}{2} \int_{\Omega} (\boldsymbol{\sigma} - \boldsymbol{\sigma}^h)^T \mathbf{D}^{-1} (\boldsymbol{\sigma} - \boldsymbol{\sigma}^h) d\Omega \right\}^{1/2}, \quad (20)$$

with the elastic constitutive matrix being

$$\mathbf{D} = \frac{E}{1-\nu^2} \begin{bmatrix} 1 & \nu & 0 \\ \nu & 1 & 0 \\ 0 & 0 & (1-\nu)/2 \end{bmatrix} \quad \text{for plane stress.} \quad (21)$$

Apart from validation exercises the exact stress  $\boldsymbol{\sigma}$  is unknown and instead a reference or projected stress must be used. For the EFGM, Chung and Belytscho [42] proposed a simple way to determine a suitable “projected” stress  $\boldsymbol{\sigma}^p$  by

$$\|e_\sigma\| \approx \|E_g\| = \left\{ \frac{1}{2} \int_{\Omega} (\boldsymbol{\sigma}^p - \boldsymbol{\sigma}^h)^T \mathbf{D}^{-1} (\boldsymbol{\sigma}^p - \boldsymbol{\sigma}^h) d\Omega \right\}^{1/2} \quad (22)$$

The “projected” stress  $\boldsymbol{\sigma}^p$  is evaluated by using an approximation at a point based on **smaller nodal supports** where

$$\boldsymbol{\sigma}^p = \sum_{k=1}^m \Psi_k(\mathbf{x}) \boldsymbol{\sigma}^h(\mathbf{x}_k), \quad (23)$$

in which  $m$  is the number of surrounding nodes **which affect the point  $\mathbf{x}$  with smaller supports** and  $\boldsymbol{\sigma}^h(\mathbf{x}_k)$  is the calculated stress vector at node  $k$  (define surrounding, is  $\boldsymbol{\sigma}^h(\mathbf{x}_k)$  the approx

stress vector at node  $k$ ?) and  $\Psi_k(\mathbf{x})$  are the shape functions obtained with this smaller support. This procedure is relatively inexpensive since there is no need for **matrix solution procedure (is this correct, still need inversion to obtain  $\Psi_k$  do we not?)**, a feature of some other error estimation procedures for meshless methods, e.g. [43, 44].

The EFGM uses a grid of integration cells to determine contributions to the domain stiffness matrix and it is convenient to arrange nodes at vertices of grid cells for the adaptive procedure. Error is estimated for each cell with subdomain  $\Omega_i$  from

$$\|E_i\| = \left\{ \frac{1}{2} \int_{\Omega_i} (\boldsymbol{\sigma}^p - \boldsymbol{\sigma}^h)^T \mathbf{D}^{-1} (\boldsymbol{\sigma}^p - \boldsymbol{\sigma}^h) d\Omega_i \right\}^{1/2}. \quad (24)$$

The accuracy of the current solution can be evaluated by a relative error measure  $\eta_g$  which is defined as

$$\eta_g = \frac{\|E_g\|}{\|U\|}, \quad (25)$$

with

$$\|U\| = \left\{ \frac{1}{2} \int_{\Omega} (\boldsymbol{\sigma}^h)^T \mathbf{D}^{-1} \boldsymbol{\sigma}^h d\Omega \right\}^{1/2}. \quad (26)$$

The adaptivity process is applied when the global error is above the target error (**this was less than in the original paper which does not sound right;**)(if it was less than, there is no need for adaptivity since the global error is small)  $\eta_g > \eta_t$ . The relative error attributed to each cell can be evaluated as

$$\eta_i = \frac{\|E_i\|}{\|U\| / \sqrt{n_{\text{cell}}}}, \quad (27)$$

where  $n_{\text{cell}}$  is the total number of cells. Predefined threshold error levels drive refinement and recovery (i.e. the opposite of refinement) by

$$\begin{cases} \eta_i > L_{\text{fin}} & \text{to be refined,} \\ \eta_i < L_{\text{rec}} & \text{to be recovered,} \end{cases} \quad (28)$$

where  $L_{\text{fin}}$  and  $L_{\text{rec}}$  are the refinement and recovery limits respectively defined according to the target error. Two steps of adaptivity are suggested: if the global error is much larger than the target error, a ‘‘coarse’’ adaptivity is adopted with a lower adaptivity requirement so more cells are considered. If the global error is close to the target error, a ‘‘fine’’ adaptivity is taken with higher adaptivity requirement. This is achieved by the following:

$$\begin{cases} L_{\text{fin}} = \alpha_1 \eta_t, L_{\text{rec}} = \beta_1 \eta_t & \text{if } \gamma \eta_t < \eta_i, \\ L_{\text{fin}} = \alpha_2 \eta_t, L_{\text{rec}} = \beta_2 \eta_t & \text{if } \eta_t < \eta_i \leq \gamma \eta_t. \end{cases} \quad (29)$$

These constants are defined according to the accuracy needed, and typical values have been found to be  $\alpha_1 = 2$ ,  $\beta_1 = 0.5$ ,  $\alpha_2 = 2.5$ ,  $\beta_2 = 0.3$ ,  $\gamma = 1.3$  and  $\eta_t = 0.08$ .

#### 4.1. Adaptive strategy

Where  $h$ -adaptivity has been used with meshless methods in the past, refinement strategies can be sub-divided on the basis of the integration method employed. Specifically, for those using Gaussian integration, the original cell is usually divided into four small cells with five nodes added as in [29, 34, 31, 32]. By contrast, for those studies based on Voronoi integration cells, nodal refinement takes place by the addition of nodes on the cell edges and the updating of surrounding Voronoi cells [45, 35]. Note that a recovery procedure is proposed in Lee *et al.* [29] to combine the four small cells into the ‘‘mother’’ cell during the crack propagation process, an approach adopted in this work to control the number of degrees of freedom. The whole procedure of adaptivity is illustrated in Fig. 7.

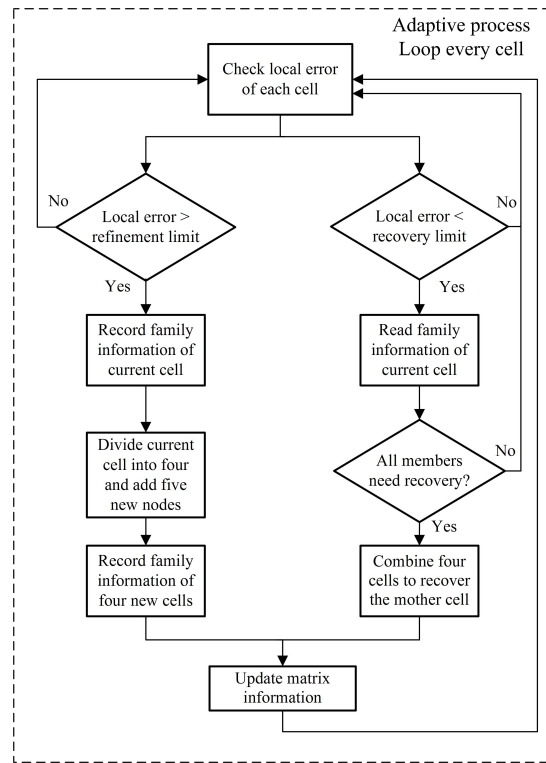


Figure 7. The flow chart of adaptivity process

The strategy of adaptivity for the new CPM presented here is shown in Fig. 8, by which new nodes are added or old nodes are deleted. For example, if the error of cell 1 is larger than  $L_{fin}$ , it is divided into four small cells, 1, 2, 3 and 4, which are recorded in a *family* matrix as a family. Further refinement of cell 2, leads to four new smaller cells 2, 5, 6 and 7, which are also recorded in the *family* matrix. Cells 1 and 2 inherit the index of the “mother” cell, which will be used if there is subsequent recovery. When four family members, cells 2, 5, 6 and 7, all have smaller errors than  $L_{rec}$ , these four cells will be recovered into the “mother” cell 2. And for further recovery, cells 1, 2, 3 and 4 will be recovered into their “mother” cell 1.

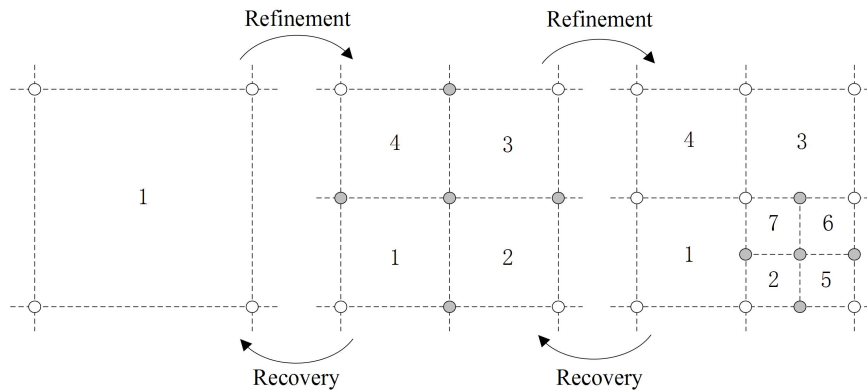


Figure 8. The strategy of refinement and recovery

For a good balance of accuracy and efficiency, nodal support sizes should be set up according to the density of surrounding nodes. When the background cells change their size during the adaptivity process, the support size of nodes should change correspondingly, the whole process

is illustrated in Fig. 9. If a cell with refinement level  $l_r$  is flagged for refinement, five nodes are added with support  $r_i = r_0 \cdot 0.5^{l_r+1}$ , where  $i=5, 6, 7, 8$  and  $9$  and  $r_0$  is the support size of initial nodes, while the four nodes ( $1, 2, 3$  and  $4$ ) of the cell need to change their support size with  $r_i = r_i \cdot \sqrt[4]{0.5}$ ,  $i=1, 2, 3$  and  $4$ . If four cells around node 1 are all refined, for example, its support size becomes the same as that of five added nodes ( $5, 6, 7, 8$  and  $9$ ). The recovery process works in an opposite way to the refinement process, with  $r_i = r_i / \sqrt[4]{0.5}$ ,  $i=1, 2, 3$  and  $4$ . The nodes in the set  $5, 6, 7, 8$  and  $9$ , which do not belong to other cells, are deleted. In the initial configuration, all nodes are almost uniformly distributed with the same support size  $r_0$  and all cells are defined with refinement level  $l_r = 0$ .

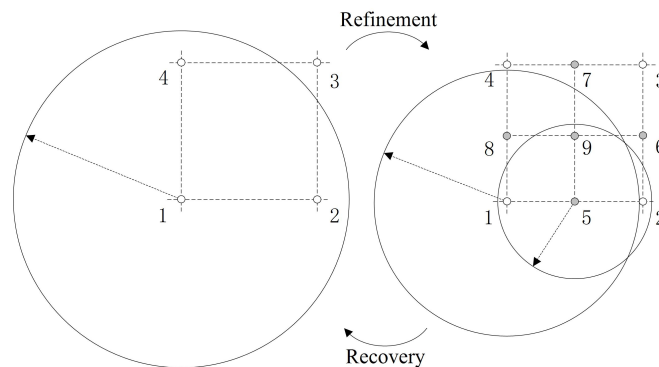


Figure 9. The change of nodal support size due to refinement and recovery

#### 4.2. Amending the stiffness matrix

Calculations using the new CPM can be accelerated by calculating and storing the system stiffness at cell level as in [46]. In this way, there is no need to reform the large system matrix frequently. The contribution of each cell to the system stiffness can be stored in a small local matrix, which makes the storage inexpensive. A *transfer* function is defined to transfer the local stiffness matrix into the system form as in Fig. 10. The local matrix of each cell can be obtained by looping over all Gauss points in the cell to evaluate the integration. All nodes involved have local index  $i$  and system index  $v(i)$ , where  $i = 1, 2, \dots, n$  where  $n$  is the number of nodes. When nodes are added or deleted during the adaptivity and crack propagation process, the vector  $v(i)$  will be updated accordingly.

When adaptivity or crack propagation occurs, only the contribution of influenced cells is required to be recalculated and the remainder can be read directly from storage. Since each propagation step leads to changes in a small zone, only a few cells need to be recalculated for each step, which reduces the computational expense of the whole process. The influenced domain for adaptivity can be determined by summing the support of deleted and added nodes as in Fig. 11, and those nodes changing their support will be considered in the two groups. By contrast, for the crack propagation process, a new cracking segment is introduced which cuts the support of some nodes as in Fig. 12. The influence domain is the combination of all shadow areas, but it is difficult to describe the influenced domain explicitly. An alternative is to use the “possible” domain, which contains all possible shadow areas. Then the system stiffness matrix can be obtained as

$$\mathbf{K} = \sum_{i \in \Omega_1} \mathcal{T}(\mathbf{k}(i)^{\text{new}}) + \sum_{j \in \Omega_2} \mathcal{T}(\mathbf{k}(j)^{\text{old}}), \quad (30)$$

where  $\mathbf{K}$  is the system stiffness matrix,  $\mathbf{k}$  is the local matrix and  $\mathcal{T}$  is the *transfer* function and the superscripts *new* and *old* indicate the state after and before the change due to the adaptivity or crack propagation respectively. When the domain  $\Omega_1$  is small, the system stiffness

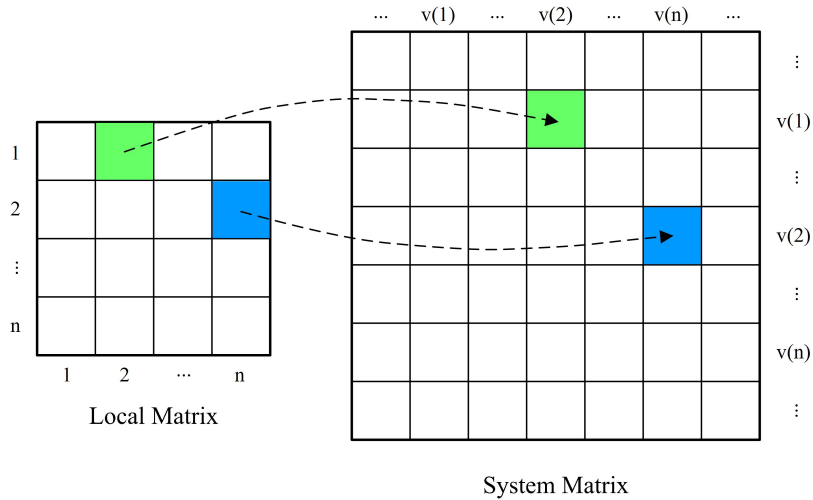


Figure 10. Transfer the local stiffness matrix into the system form

matrix can be obtained by

$$\mathbf{K} = \mathbf{K}^{\text{old}} - \sum_{i \in \Omega_1} \mathcal{T}(\mathbf{k}(i)^{\text{old}}) + \sum_{i \in \Omega_1} \mathcal{T}(\mathbf{k}(i)^{\text{new}}) . \quad (31)$$

Here, the matrix operation should be adopted to change the old form matrix to the new form so that they have the same degree. The whole analysis process is illustrated in Fig. 13.

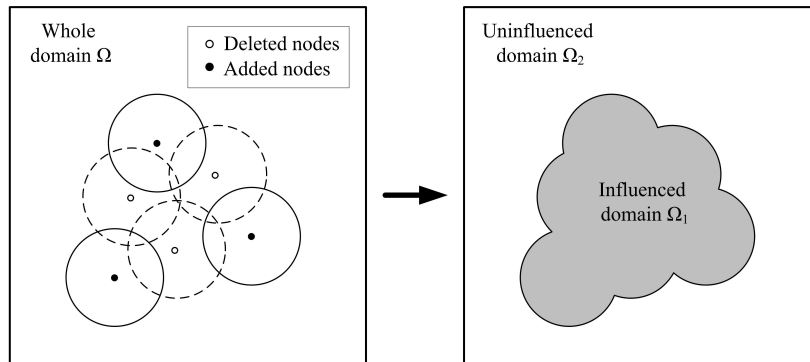


Figure 11. Influenced domain due to adaptivity

## 5. NUMERICAL EXAMPLES

Several 2D crack problems are now presented to demonstrate the performance of the proposed CPM, and in all examples plane stress conditions and elastic material properties are assumed. For all examples, a linear basis is used to build the shape functions and  $4 \times 4$  Gauss points are applied to evaluate stiffness contributions in each cell. All the problems are assumed to be subject to quasi-static loading and only the propagating path of cracks is studied, so the critical  $K_I$  is set to a low value with  $K_{IC} = 1000\text{N}/\text{mm}^{3/2}$ . The initial support size is  $r_0 = 2l_c$ , where  $l_c$  is the average length of cell edges at the start, where the factor of 2 is chosen within the range 2.0 - 4.0 following the advice in [47, 41], and the projected support size in the error estimation part is  $r = 0.8r_i$ , where  $r_i$  is the support of node  $i$ .

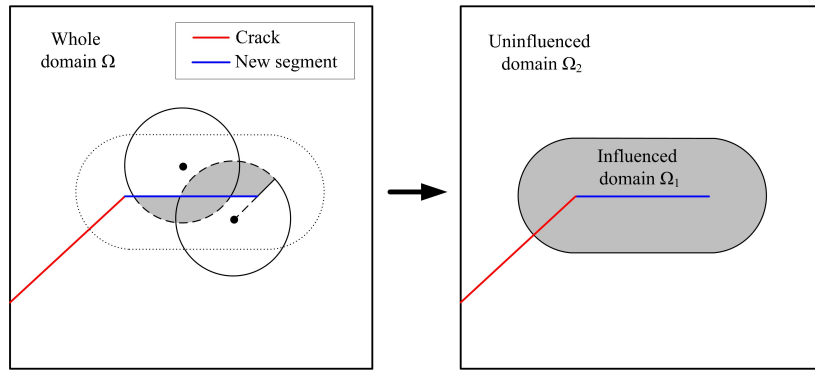


Figure 12. Influenced domain due to crack propagation

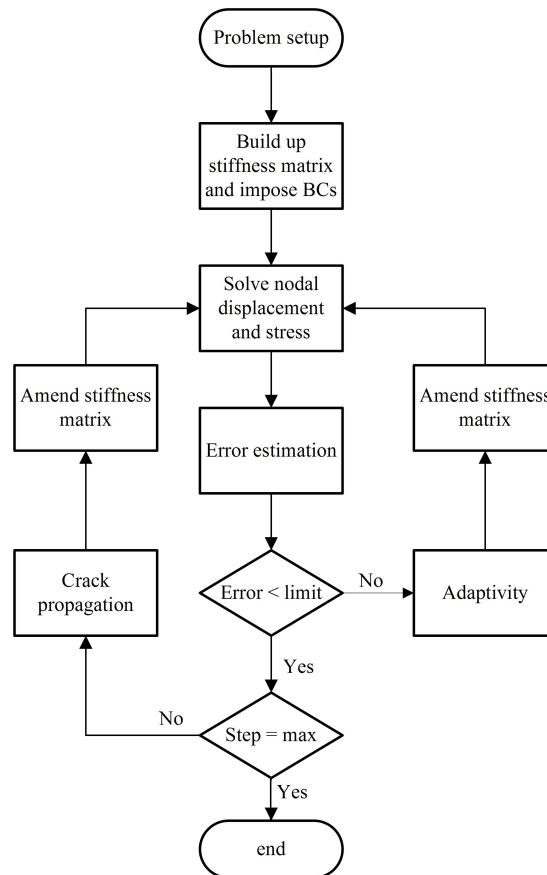


Figure 13. The flow chart of whole analysis process

### 5.1. An edge crack

The first example is a simple problem, the edge crack, but there are theoretical solutions which can be used to test the accuracy of the proposed methodology. The geometry of edge crack problem is shown in Fig. 14 with  $a = 20$  mm,  $b = 100$  mm and  $h = 100$  mm. The plate is loaded by a uniform force  $q = 100$  N/mm and the material properties are  $E = 74$  GPa and  $\nu = 0.3$ . The adaptivity input parameters are set with  $\alpha_1 = 2$ ,  $\beta_1 = 0.5$ ,  $\alpha_2 = 2.5$ ,  $\beta_2 = 0.3$ ,  $\gamma = 1.3$  and  $\eta_t = 0.08$ , and the maximum refinement level is 6 so the smallest distance between nodes

is  $2^{-6}r_0 = r_0/64$ . The problem is symmetric so the crack will propagate horizontally without considering the change of cracking angle.

The adaptive process combined with the crack propagation is presented in Fig. 15, in which the mass of nodes moves with the crack tip travelling. The whole process is controlled by the *refinement* function to add nodes around the crack tip and by the *recovery* function to delete nodes around the old crack tip in the previous steps. The mode I SIF is extracted through the domain integration as mentioned above and is compared with exact values as in [48] by

$$K_I = q\sqrt{\pi a} \left[ 1.122 - 0.231\left(\frac{a}{b}\right) + 10.550\left(\frac{a}{b}\right)^2 - 21.710\left(\frac{a}{b}\right)^3 + 30.382\left(\frac{a}{b}\right)^4 \right]. \quad (32)$$

As shown in Fig. 16, good results can be obtained during the crack propagation process and node arrangements are set up automatically to guarantee the efficiency and accuracy.

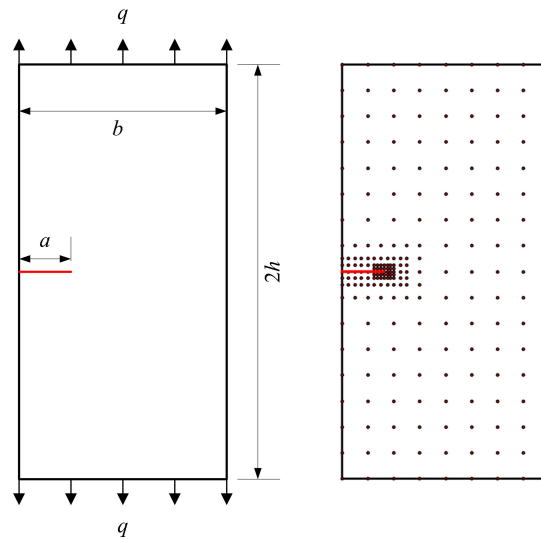


Figure 14. Configuration and initial nodes of edge crack

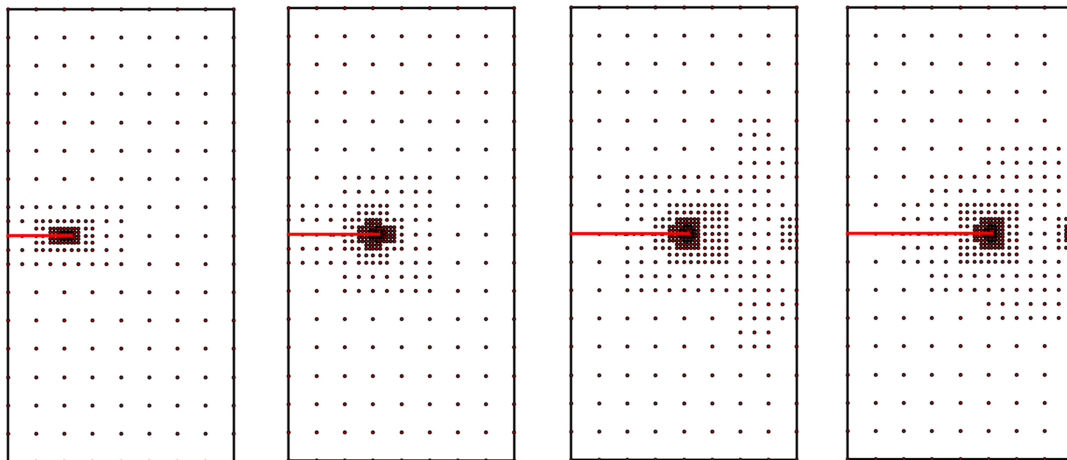


Figure 15. Crack propagation and corresponding nodal arrangement (steps 3, 6, 9, 12)

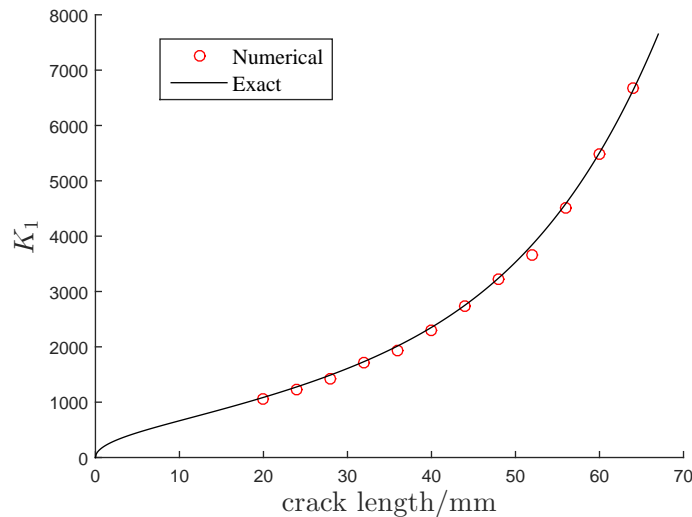


Figure 16. Comparison between calculated mode I stress intensity factor with theoretic solutions

### 5.2. A double cantilever beam

The second example, the double cantilever beam, is more complex than the first one and the change of cracking angle is considered. The geometry of double cantilever beam is depicted in Fig. 17 with  $L = 30$  cm,  $h = 10$  cm,  $a = 10$  cm,  $\Delta x = 0.76$  cm and  $d\theta = 0.1$ , with the same specimen as in [29]. The material properties are  $E = 206.8$  GPa and  $\nu = 0.3$ . The adaptivity input parameters are set with  $\alpha_1 = 2$ ,  $\beta_1 = 0.5$ ,  $\alpha_2 = 2.5$ ,  $\beta_2 = 0.3$ ,  $\gamma = 1.3$  and  $\eta_t = 0.08$ , and the maximum refinement level is 6. The right side of beam is fully clamped while the left side is loaded by two groups of traction with  $q = 175$  N/cm.

The whole crack propagation process is shown in Fig. 18 and the crack direction changes from horizon to vertical due to the perturbation at the crack tip. There is also a mass of nodes travelling with the crack tip, which is controlled by the adaptivity approach. When the crack propagates, fine nodes are added around the crack tip while those far away from the tip are recovered. Note that since the crack is simulated by discrete segments, fine node arrangements are required around crack path where there is a sudden change, which therefore are not recovered. The maximum number of nodes is 970, compared to initial nodal number 397. The predicted crack path shows good agreements with previous results [29] as shown in Fig. 19.

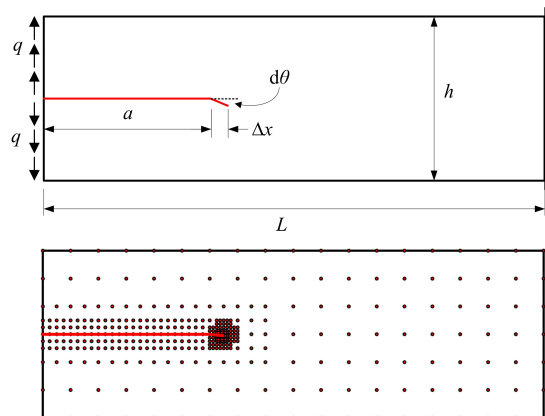


Figure 17. Configuration and initial nodes of Double Cantilever Beam

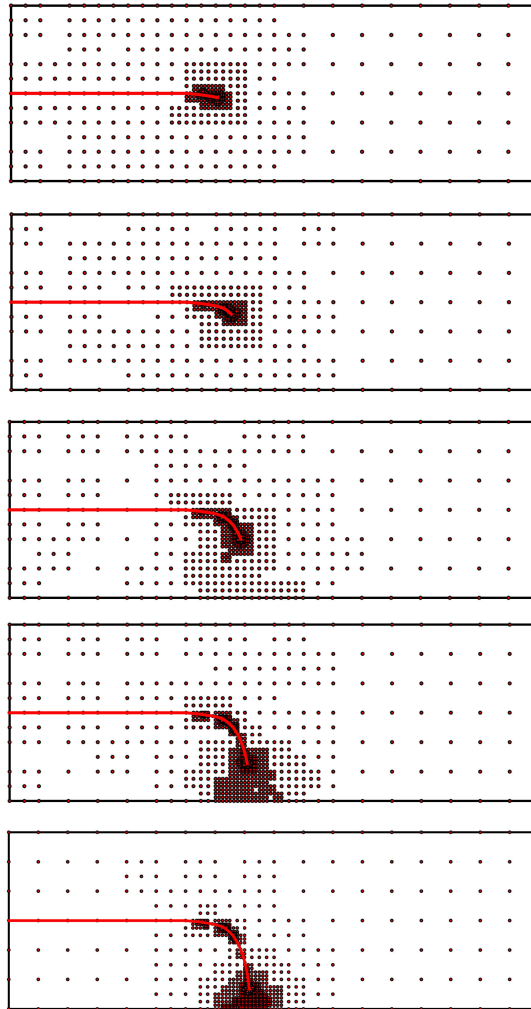


Figure 18. Crack propagation and corresponding nodal arrangement (steps 5, 10, 15, 20 and 24)

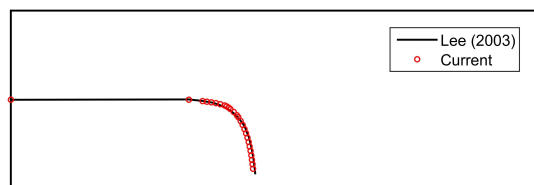


Figure 19. Predicted crack propagation compared with previous results

### 5.3. Multiple cracks in a plate with two holes

The last example is the most challenging problem, where multiple cracks are considered. And there are two holes in the plate, so elements around the hole are no longer square. The geometry of this problem is illustrated in Fig. 20, which is the same as [49, 50]. Particularly,  $L = 20$  mm,  $h = 10$  mm,  $a = 1$  mm,  $h_0 = 2.85$  mm,  $R = 2$  mm and  $d = 3$  mm. The top and down sides of the plate are both loaded by a uniform tensile and the value of force is not mentioned in [49]. Here the load is achieved by fixing the down side and giving the top side a displacement with  $0.02h$  to approximate the original problem. The adaptivity input parameters are set with

$\alpha_1 = 2$ ,  $\beta_1 = 0.4$ ,  $\alpha_2 = 1.6$ ,  $\beta_2 = 0.8$ ,  $\gamma = 1.2$  and  $\eta_t = 0.08$ , and the maximum refinement level is 5. The whole crack propagation process is shown in Fig. 21, and there are two groups

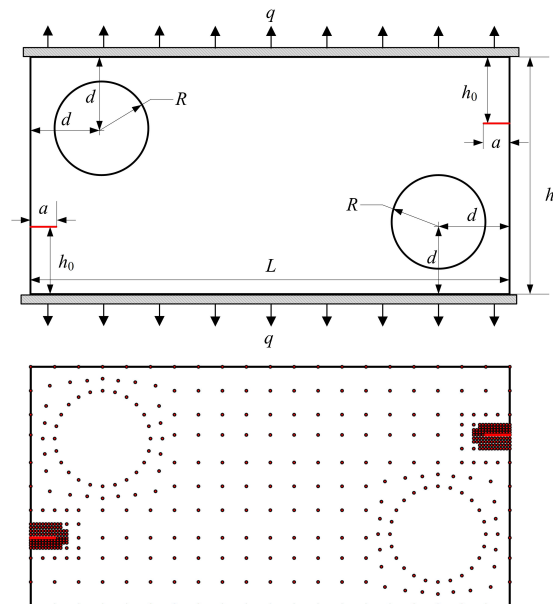


Figure 20. Configuration and initial nodes of multiple-crack problem

of fine nodes around both crack tips, travelling with cracks propagating. The two cracks firstly propagate towards the nearest hole to themselves, then both of them change the cracking angle horizontally until they meet each other in the centre of plate. The two cracks are attracted by each other and propagate closely to the opposing crack. Finally, two cracks are attracted by the hole which was far from them and move towards it. During this process, the adaptivity approach controls the node arrangements around two crack tips and the maximum number of nodes is 4372, which is nearly 8 times larger than initial nodal number 532. The predicted crack path is compared with previous results in [49] and good agreements are achieved as in Fig. 22.

The proposed adaptive CPM shows good performance when solving fracture problems as shown above. Currently, the crack branching problems, which were mentioned in Rabzuk's paper [11], are complex for the adaptivity process, so they are not included in this work. But the CPM has shown the ability to handle multiple-crack problems and crack branching problems and solving a large number of cracks at the same time becomes possible with the proposed methodology, which is one of the tasks for future research.

## 6. CONCLUSIONS

In this paper, an adaptive Cracking Particle Method is developed for 2D quasi-static crack propagation analysis. The crack is described by discrete segments and can be easily updated by adding cracking particles, which makes this methodology much simpler than methods based on level sets and can be used to handle multiple crack problems. The density and support size of nodes are controlled by the adaptivity approach to make sure the whole analysis is accurate and efficient. The discrete segments are achieved through cracking particles with broken lines but not by straight lines, so they barely cross with each other and there is no spurious cracking. The broken lines can record the angular change of crack propagation, which makes it suitable to describe discontinuous cracks. Calculating and storing the system stiffness at cell level is introduced into the adaptivity to accelerate the whole process. In this way, only

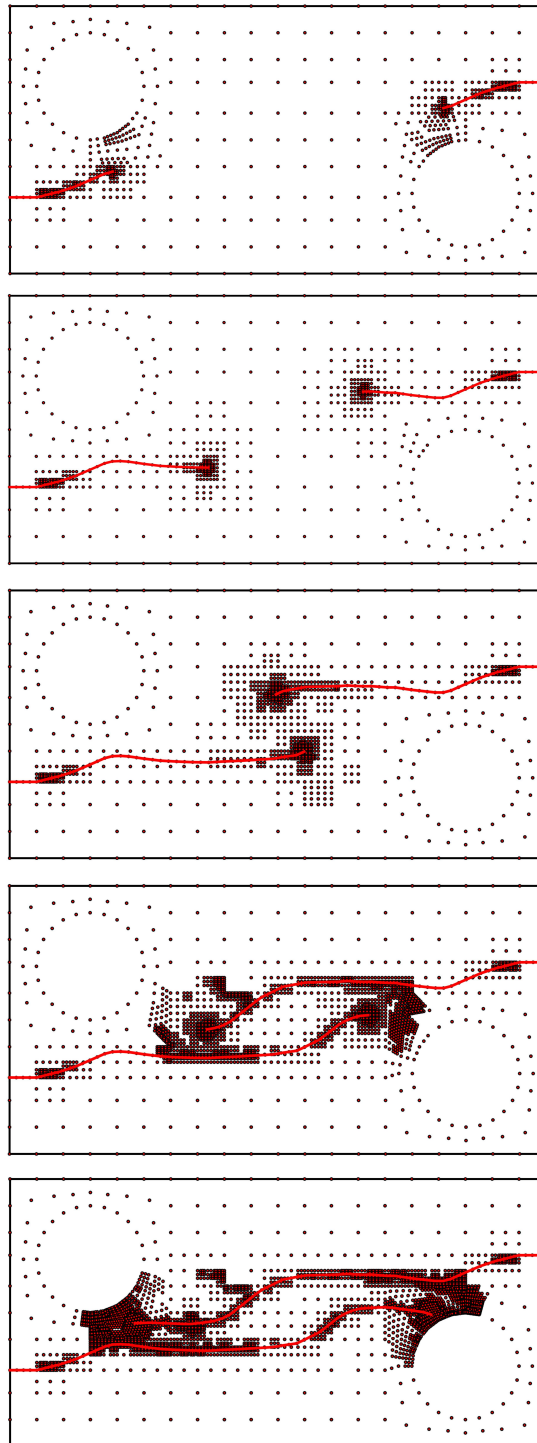


Figure 21. Adaptive process of multiple-crack problem with steps 7, 14, 21, 28 and 33

a small influenced domain is required to be calculated for each step while the remainder can be read directly from the storage, which highly reduces the cost of the whole calculation. This approach can also be applied to other kinds of adaptivity process as a kind of acceleration. Some numerical examples are carried out to explore the performance of the proposed methodology and good agreements are obtained. In the last example, the proposed methodology is used to

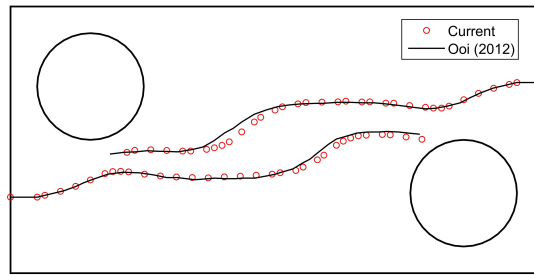


Figure 22. Comparison between predicted crack path and previous result

solve a problem with two cracks, which shows its potential to handle more complex problems and the crack branching will be considered in future work.

#### ACKNOWLEDGEMENT

The first author would like to thank the China Scholarship Council(CSC) and the Faculty of Science, Durham University for funding his PhD study at Durham University.

## REFERENCES

1. Xu X, Needleman A. Numerical simulations of dynamic crack growth along an interface. *International Journal of Fracture* 1995; **74**(4):289–324.
2. Ortiz M, Pandolfi A. Finite-deformation irreversible cohesive elements for three-dimensional crack-propagation analysis. *International Journal for Numerical Methods in Engineering* 1999; **44**(9):1267–1282.
3. Moës N, Gravouil A, Belytschko T. Non-planar 3d crack growth by the extended finite element and level setspart i: Mechanical model. *International Journal for Numerical Methods in Engineering* 2002; **53**(11):2549–2568.
4. Gravouil A, Moës N, Belytschko T. Non-planar 3d crack growth by the extended finite element and level setspart ii: Level set update. *International Journal for Numerical Methods in Engineering* 2002; **53**(11):2569–2586.
5. Duffot M. A study of the representation of cracks with level sets. *International Journal for Numerical Methods in Engineering* 2007; **70**(11):1261–1302.
6. Zhuang X, Augarde C, Bordas S. Accurate fracture modelling using meshless methods, the visibility criterion and level sets: formulation and 2d modelling. *International Journal for Numerical Methods in Engineering* 2011; **86**(2):249–268.
7. Zhuang X, Augarde C, Mathisen K. Fracture modeling using meshless methods and level sets in 3d: framework and modeling. *International Journal for Numerical Methods in Engineering* 2012; **92**(11):969–998.
8. Belytschko T, Gu L, Lu Y. Fracture and crack growth by element free Galerkin methods. *Modelling and Simulation in Materials Science and Engineering* 1994; **2**(3A):519–534.
9. Belytschko T, Lu Y, Gu L. Crack propagation by element-free Galerkin methods. *Engineering Fracture Mechanics* 1995; **51**(2):295–315.
10. Belytschko T, Lu Y, Gu L, Tabbara M. Element-free Galerkin methods for static and dynamic fracture. *International Journal of Solids and Structures* 1995; **32**(17):2547–2570.
11. Rabczuk T, Belytschko T. Cracking particles: a simplified meshfree method for arbitrary evolving cracks. *International Journal for Numerical Methods in Engineering* 2004; **61**(13):2316–2343.
12. Belytschko T, Lu Y, Gu L. Element-free Galerkin methods. *International Journal for Numerical Methods in Engineering* 1994; **37**(2):229–256.
13. Thomas P, Hermann G. Classification and overview of meshfree methods. *Institute of Scientific Computing, Technical University Braunschweig, Brunswick, Germany* 2004; .
14. Rabczuk T, Belytschko T. A three-dimensional large deformation meshfree method for arbitrary evolving cracks. *Computer Methods in Applied Mechanics and Engineering* 2007; **196**(29):2777–2799.
15. Rabczuk T, Zi G, Bordas S, Nguyen-Xuan H. A simple and robust three-dimensional cracking-particle method without enrichment. *Computer Methods in Applied Mechanics and Engineering* 2010; **199**(37):2437–2455.
16. Kumar V, Ghosh A. Modeling of dynamic fracture based on the cracking particles method. *THEORETICAL AND APPLIED FRACTURE MECHANICS* FEB 2015; **75**:22–31, doi:{10.1016/j.tafmec.2014.10.003}.
17. Ghosh A, Kumar Vz. Computational studies on fragmentation of brittle materials. *PROCEEDINGS OF THE INSTITUTION OF MECHANICAL ENGINEERS PART C-JOURNAL OF MECHANICAL ENGINEERING SCIENCE* AUG 2013; **227**(8):1650–1664, doi:{10.1177/0954406212466766}.
18. Chen L, Zhang YY. Dynamic fracture analysis using discrete cohesive crack method. *INTERNATIONAL JOURNAL FOR NUMERICAL METHODS IN BIOMEDICAL ENGINEERING* NOV 2010; **26**(11):1493–1502, doi:{10.1002/cnm.1232}.
19. Kumar V, Drathi R. A meshless Cracking Particles Approach for ductile fracture. *KSCE JOURNAL OF CIVIL ENGINEERING* JAN 2014; **18**(1):238–248, doi:{10.1007/s12205-014-0164-4}.
20. Xu S. Stable Cracking Particles Method Based on Stabilized Nodal Integration and Updated Lagrangian Kernel. *MATHEMATICAL PROBLEMS IN ENGINEERING* 2014; doi:{10.1155/2014/646514}.
21. Organ D, Fleming M, Terry T, Belytschko T. Continuous meshless approximations for nonconvex bodies by diffraction and transparency. *Computational Mechanics* 1996; **18**(3):225–235.
22. Rice JR. A path independent integral and the approximate analysis of strain concentration by notches and cracks. *Journal of Applied Mechanics* 1968; **35**(2):379–386.
23. Yan A, Nguyen-Dang H. Multiple-cracked fatigue crack growth by BEM. *Computational Mechanics* 1995; **16**(5):273–280.
24. Berković M. Determination of stress intensity factors using finite element method. *Structural integrity and life* 2004; **4**(2).
25. Yau J, Wang S, Corten H. A mixed-mode crack analysis of isotropic solids using conservation laws of elasticity. *Journal of Applied Mechanics* 1980; **47**(2):335–341.
26. Yu H, Wu L, Guo L, Du S, He Q. Investigation of mixed-mode stress intensity factors for nonhomogeneous materials using an interaction integral method. *International Journal of Solids and Structures* 2009; **46**(20):3710–3724.
27. Bouchard PO, Bay F, Chastel Y. Numerical modelling of crack propagation: automatic remeshing and comparison of different criteria. *Computer methods in applied mechanics and engineering* 2003; **192**(35):3887–3908.
28. Erdogan F, Sih G. On the crack extension in plates under plane loading and transverse shear. *Journal of Fluids Engineering* 1963; **85**(4):519–525.
29. Lee GH, Chung HJ, Choi CK. Adaptive crack propagation analysis with the element-free Galerkin method. *International Journal for Numerical Methods in Engineering* 2003; **56**(3):331–350.

30. Rossi R, Alves MK. An h-adaptive modified element-free Galerkin method. *European Journal of Mechanics-A/Solids* 2005; **24**(5):782–799.
31. Ullah Z, Augarde C. Finite deformation elasto-plastic modelling using an adaptive meshless method. *Computers & Structures* 2013; **118**:39–52.
32. Ullah Z, Coombs W, Augarde C. An adaptive finite element/meshless coupled method based on local maximum entropy shape functions for linear and nonlinear problems. *Computer Methods in Applied Mechanics and Engineering* 2013; **267**:111–132.
33. Häussler-Combe U, Korn C. An adaptive approach with the element-free-Galerkin method. *Computer Methods in Applied Mechanics and Engineering* 1998; **162**(1):203–222.
34. Rabczuk T, Belytschko T. Adaptivity for structured meshfree particle methods in 2d and 3d. *International Journal for Numerical Methods in Engineering* 2005; **63**(11):1559–1582.
35. Le CV, Askes H, Gilbert M. Adaptive element-free Galerkin method applied to the limit analysis of plates. *Computer Methods in Applied Mechanics and Engineering* 2010; **199**(37):2487–2496.
36. Zienkiewicz O, Boroomand B, Zhu J. Recovery procedures in error estimation and adaptivity part i: Adaptivity in linear problems. *Computer Methods in Applied Mechanics and Engineering* 1999; **176**(1):111–125.
37. Boroomand B, Zienkiewicz O. Recovery procedures in error estimation and adaptivity. part ii: Adaptivity in nonlinear problems of elasto-plasticity behaviour. *Computer Methods in Applied Mechanics and Engineering* 1999; **176**(1):127–146.
38. Duarte CA, Oden JT. An h-p adaptive method using clouds. *Computer Methods in Applied Mechanics and Engineering* 1996; **139**(1):237–262.
39. Krysl P, Belytschko T. Element-free Galerkin method: Convergence of the continuous and discontinuous shape functions. *Computer Methods in Applied Mechanics and Engineering* 1997; **148**(3):257–277.
40. Fleming M, Chu Y, Moran B, Belytschko T, Lu Y, Gu L. Enriched element-free Galerkin methods for crack tip fields. *International Journal for Numerical Methods in Engineering* 1997; **40**(8):1483–1504.
41. Zhuang X, Heaney C, Augarde C. On error control in the element-free galerkin method. *Engineering Analysis with Boundary Elements* 2012; **36**(3):351 – 360, doi:<http://dx.doi.org/10.1016/j.enganabound.2011.06.011>. URL <http://www.sciencedirect.com/science/article/pii/S0955799711001445>.
42. Chung HJ, Belytschko T. An error estimate in the EFG method. *Computational Mechanics* 1998; **21**(2):91–100.
43. Lee CK, Zhou C. On error estimation and adaptive refinement for element free galerkin method: Part i: stress recovery and a posteriori error estimation. *Computers & structures* 2004; **82**(4):413–428.
44. Lee C, Zhou C. On error estimation and adaptive refinement for element free galerkin method: Part ii: adaptive refinement. *Computers & structures* 2004; **82**(4):429–443.
45. You Y, Chen JS, Lu H. Filters, reproducing kernel, and adaptive meshfree method. *Computational Mechanics* 2003; **31**(3-4):316–326.
46. Peco C, Millán D, Rosolen A, Arroyo M. Efficient implementation of Galerkin meshfree methods for large-scale problems with an emphasis on maximum entropy approximants. *Computers & Structures* 2015; **150**:52–62.
47. Dolbow J, Belytschko T. An introduction to programming the meshless element free Galerkin method. *Archives of Computational Methods in Engineering* 1998; **5**(3):207–241.
48. Tada H, Paris P, Irwin G. The analysis of cracks handbook. *New York: ASME Press* 2000; .
49. Ooi ET, Song C, Tin-Loi F, Yang Z. Polygon scaled boundary finite elements for crack propagation modelling. *International journal for numerical methods in engineering* 2012; **91**(3):319–342.
50. Dai S, Augarde C, Du C, Chen D. A fully automatic polygon scaled boundary finite element method for modelling crack propagation. *Engineering Fracture Mechanics* 2015; **133**:163–178.